Compressed Sensing in MRI with a Markov Random Field prior for spatial clustering of subband coefficients

Marko Panić*, Jan Aelterman†, Vladimir Crnojević* and Aleksandra Pižurica†
*University of Novi Sad, BioSense Institute
mpanic@uns.ac.rs, crnjvc@gmail.com
†Ghent University, Department Telecommunications and Information Processing, TELIN-IPI-iMinds
Jan.Aelterman@ugent.be, Aleksandra.Pizurica@ugent.be

***Abstract*—Recent work in compressed sensing of magnetic resonance images (CS-MRI) concentrates on encoding structured sparsity in acquisition or in the reconstruction stages. Subband coefficients of typical images obey a certain structure, which can be viewed in terms of fixed groups (like wavelet trees) or statistically (certain configurations are more likely than others). Approaches using wavelet tree-sparsity have already demonstrated excellent performance in MRI. However, the use of statistical models for spatial clustering of the subband coefficients has not been studied well in CS-MRI yet, although the potentials of such an approach have been indicated. In this paper, we design a practical reconstruction algorithm as a variant of the proximal splitting methods, making use of a Markov Random Field prior model for spatial clustering of subband coefficients. The results for different undersampling patterns demonstrate an improved reconstruction performance compared to both standard CS-MRI methods and methods based on wavelet tree sparsity.**

I. Introduction

Reconstruction of magnetic resonance (MR) images from compressively sensed partial Fourier data is an ill-posed linear inverse problem (ILIP)

$$\mathbf{y} = \mathbf{A}\mathbf{x} + \mathbf{n} \tag{1}$$

where $\mathbf{x} \in \mathbb{C}^N$ denotes the MR image and $\mathbf{y} \in \mathbb{C}^M$ are incomplete measurements obtained through partially observed Fourier transform $\mathbf{A} \in \mathbb{C}^{M\times N}, M \ll N$ with added noise $\mathbf{n} \in \mathbb{C}^M$ [1], [2]. The measurement matrix $\mathbf{A}$ models the process of acquiring partial MR image data in the frequency domain *i.e.*, in the so called k-space. In this setting, the use of Compressed Sensing (CS) tools to recover the underlying MR image (MRI) is referred to as CS-MRI. Solving the under determined system in (1) requires some form of regularization. CS-MRI approaches make use of the fact that typical MR images are compressible under a well chosen sparsyfying transform (such as wavelet-like transforms). Denoting the sparsifying transform by $\mathbf{P} \in \mathbb{C}^{D\times N}$, the problem in (1) can be regularized as constrained optimization [3], [4]:

$$\min_{\mathbf{x}\in\mathbb{C}^N} \phi(\mathbf{P}\mathbf{x}) \quad \text{subject to} \quad \|\mathbf{A}\mathbf{x} - \mathbf{y}\|_2^2 \leq \epsilon \tag{2}$$

where $\phi : \mathbb{C}^D \mapsto \mathbb{R}\cup\{-\infty, +\infty\}$ is a regularization function, applied here to the image coefficients $\boldsymbol{\theta} = \mathbf{P}\mathbf{x}$, and $\epsilon \geq 0$ is a parameter, which depends on the noise variance. Choosing ℓ_1 ($\phi(\boldsymbol{\theta}) = ||\boldsymbol{\theta}||_1$) norm as the regularization function leads to the basis pursuit denoising (BPDN) problem [5]. Another common regularization in image recovery problems is Total Variation (TV), where the sparsifying transform $\mathbf{P}$ is a discrete gradient operator. CS-MRI approaches often employ compound regularization too (as a combination of TV and ℓ_1 norm of the wavelet-like coefficients) [1], [2], [6], [7].

Numerous algorithms for solving (2) can be categorized into (i) *greedy* methods, such as compressive sampling matching pursuit (CoSaMP) [8], subspace pursuit (SP) [9] and Iterative Hard Thresholding (IHT) [10], [11] and (ii) *convex optimization*-based methods, including fast proximal gradient methods (FISTA) [12] with extensions [6], [13] and variants of the Augmented Lagrangian (AL) method such as alternating direction method of multipliers (ADMM) [4] and equivalent formulations [14], [15].

Recent research shows benefits of modelling *structure* of the sparse, information-bearing coefficients either in the acquisition [16] or in the reconstruction [17] stages. Improved CS-MRI reconstruction making use of the wavelet tree structure was recently reported in [18], [19]. In contrast to these methods, which model the *inter-scale* dependencies among the wavelet coefficients, the so-called Lattice Matching Pursuit (LaMP) algorithm of [20] models the *intra-scale* coefficient dependencies, by encoding spatial clustering of the coefficients within each subband with a Markov Random Field. LaMP demonstrated superior performance in background subtraction but was not evaluated in MRI to our knowledge yet. A related method of [21] named by analogy with LaMP as Lattice Split Bregman (LaSB) incorporated MRF-based support estimation within the augmented Lagrangian approach. Although the presentation of LaSB was rather heuristic (component-wise soft-thresholding step from the original algorithm was simply replaced by a lattice selector), the results indicated a great potential for MRI reconstruction.

Motivated by the encouraging results of [21], we study further the potentials of MRF priors in CS-MRI. Our focus is on structure only in the recovery algorithm, with standard sampling strategies. We develop a new, practical MRI

978-0-9928-6265-7/16/$31.00 ©2016 IEEE

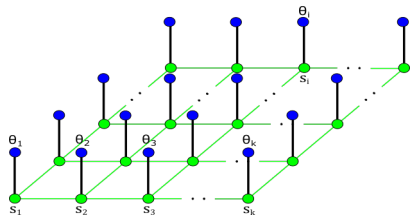

Fig. 1. A graphical representation of the MRF model for the support labelling $\mathbf{s}$ of image coefficients $\boldsymbol{\theta}$ in one subband.

reconstruction algorithm as a variant of the proximal splitting methods, employing a Markov Random Field prior in the shearlet domain. In essence, the proposed algorithm embeds a general model based sparsity framework with MRF priors [22] into a constrained split augmented Lagrangian method related to C-SALSA [4]. In comparison to the related LaSB [21], we employ not only a different optimization method, but also a more general MRF prior model (allowing different a priori probabilities of significant and insignificant coefficients), and we now motivate and present our algorithm in terms of the proximal operators. The results comply with the findings of [21] in the sense that making use of the support estimation with MRF priors enhances the performance of the underlying AL method, but the new algorithm achieves superior performance with respect to [21]. Moreover, the results show consistent improvement over the methods based on wavelet-tree sparsity [18], [19], both in terms of mean squared error and visually.

II. An MRF-based structured sparsity model

Our approach aims to incorporate efficiently Bayesian estimation of the most likely support configurations within the iterative method for solving (2). The solver will be updated to guide the solution towards feasible ones based on the estimated supports in each iteration.

A. Modelling structured supports

Given the index set $\mathcal{N} = \{1, 2, 3, ..., D\}$, let $supp(\boldsymbol{\theta}) = \{i \in \mathcal{N} : \boldsymbol{\theta}_i \neq 0\}$ denote the *support* of the sparse signal $\boldsymbol{\theta} \in \mathbb{C}^D$. A structured sparsity signal model $\mathcal{M}$ is a set of signals whose supports belong to the set of presumable *structured supports* $\mathbb{M}$ [17]. In our practical algorithm, the coefficients $\boldsymbol{\theta} = \mathbf{Px}$ are obtained using an undecimated shearlet transform [23], with the design from [24], although any other wavelet-like transform can be used instead.

Let a binary label $s_i \in \{0, 1\}$ mark the significance of the corresponding coefficient θ_i: $s_i = 1$ if θ_i is significant (*i.e.* "signal of interest") and $s_i = 0$ otherwise. We shall model plausible support configurations by treating configurations $\mathbf{s} = \{s_1, ..., s_D\}$ as realizations of a Markov Random Field $\mathbf{S} = \{S_1, ..., S_D\}$. Denote the index set corresponding to the support $\mathbf{s}$ by

$$\Omega_{\mathbf{s}} = \{i \in \mathcal{N} : s_i = 1\} \tag{3}$$

Suppose $\hat{\mathbf{s}}$ is the most likely support and define a model confined to this support as

$$\mathcal{M}_{\hat{\mathbf{s}}} = \{\boldsymbol{\theta} \in \mathbb{C}^D \mid supp(\boldsymbol{\theta}) = \Omega_{\hat{\mathbf{s}}}\}. \tag{4}$$

Utilizing this model to regularize the problem (1) leads to

$$\min_{\mathbf{x} \in \mathbb{C}^N} \|\mathbf{Ax} - \mathbf{y}\|_2^2 \quad \text{subject to} \quad \mathbf{Px} = \boldsymbol{\theta} \in \mathcal{M}_{\hat{\mathbf{s}}} \tag{5}$$

which can be considered as a type of discrete projection formulation defined in [22]. Each iteration of the algorithm for solving this problem requires the projection operator:

$$\Pi_{\mathcal{M}_{\hat{\mathbf{s}}}}(\boldsymbol{\theta}) = \underset{\boldsymbol{\gamma} \in \mathbb{C}^D}{\operatorname{argmin}} \left\{ \|\boldsymbol{\gamma} - \boldsymbol{\theta}\|_2^2 \mid supp(\boldsymbol{\gamma}) = \Omega_{\hat{\mathbf{s}}} \right\} \tag{6}$$

for which the solution $\hat{\boldsymbol{\gamma}}$ is such that $\hat{\gamma}_i = \theta_i$ if $\hat{s} = 1$ and $\hat{\gamma}_i = 0$ if $\hat{s}_i = 0$.

Our estimation of the supports $\hat{\mathbf{s}}$ will make use of the maximum a posteriori probability (MAP) criterion. In each iteration of the selected solver, we employ the temporary signal estimate $\boldsymbol{\theta}'$ to infer the most likely support in the MAP sense:

$$\hat{\mathbf{s}} = \underset{\mathbf{s}}{\operatorname{argmax}}\, P_{\mathbf{S}|\boldsymbol{\Theta}'}(\mathbf{s} \mid \boldsymbol{\theta}') = \underset{\mathbf{s}}{\operatorname{argmax}}\, p_{\boldsymbol{\Theta}'|\mathbf{S}}(\boldsymbol{\theta}' \mid \mathbf{s}) P_{\mathbf{S}}(\mathbf{s}) \tag{7}$$

Then we refine $\boldsymbol{\theta}'$ based on $\hat{\mathbf{s}}$. The particular prior and the conditional model from (7), as well as the inference algorithm for solving it are explained next.

B. MRF prior

The joint probability of a Markov Random Field $P_{\mathbf{S}}(\mathbf{s}) = P(\mathbf{S} = \mathbf{s})$ is a Gibbs distribution [25] [26]

$$P_{\mathbf{S}}(\mathbf{s}) = \frac{1}{Z} e^{-H(\mathbf{s})/T} \tag{8}$$

where the energy $H(\mathbf{s})$ is decomposed as a sum of clique potentials over all possible cliques: $H(\mathbf{s}) = \sum_{c \in \mathcal{C}} V_c(\mathbf{s})$. The partition function $Z = \sum_{\mathbf{s} \in \mathcal{S}} e^{-H(\mathbf{s})/T}$, which sums the probability over the set of all possible configurations $\mathcal{S}$ has the role of a normalization constant, while the "temperature" T controls the peaking in the probability distribution [25]. We shall use a common homogeneous model with the first-order neighbourhood, where

$$H(\mathbf{s}) = \sum_i V_1(s_i) + \sum_{\langle i,j \rangle \in \mathcal{C}} V_2(s_i, s_j) \tag{9}$$

with single and pairwise clique potentials defined as

$$V_1(s) = \begin{cases} \alpha & s = 0 \\ -\alpha & s = 1 \end{cases}, \quad V_2(s,t) = \begin{cases} -\beta & s = t \\ \beta & s \neq t \end{cases} \tag{10}$$

A similar model was used in [21], but with $\alpha = 0$. We do allow different a priori probabilities of the two types of labels $\alpha \neq 0$, to be able to affect the sparsity of the configurations. Regardless of the fraction of different label types, the strength of their spatial clustering is controlled by the parameter $\beta > 0$.

C. Conditional model

We adopt the same conditional model $p_{\boldsymbol{\Theta}|\mathbf{S}}(\boldsymbol{\theta}|\mathbf{s})$ as in [21], [26]. With the conditional independence assumption, which is common in this setting, we have $p_{\boldsymbol{\Theta}|\mathbf{S}}(\boldsymbol{\theta}|\mathbf{s}) = \prod_i p_{\Theta_i|S_i}(\theta_i|s_i)$. The observed coefficients are typically noisy versions of the ideal ones: $\theta = u + n$, where n denotes the noise component. We select the prior $p_U(u)$ as the generalized

Laplacian and we estimate its parameters from the noisy coefficient histogram, knowing the noise standard deviation σ (which is in practice reliably estimated from the empty area on the borders of the MR image and rescaled appropriately in each subband). Let T_h denote the significance threshold for the ideal noise-free coefficients (u is significant if $|u| \geq T_h$). We relate this threshold to the noise level, but in a conservative manner, such that T_h is only a fraction of σ (in practice 10%). The conditional densities $p_{U|S}(u|0)$ and $p_{U|S}(u|1)$ are then obtained by rescaling the central part ($|u| < T_h$) and the tails ($|u| \geq T_h$) of $p_U(u)$, respectively, so that they both integrate to 1. The conditional densities of the noisy coefficients $p_{\Theta|S}(\theta|s)$ are obtained from the corresponding $p_{U|S}(u|s)$. For the additive noise model $\theta = u + n$ with $n \sim N(0, \sigma)$, $p_{\Theta|S}(\theta|s)$ is simply the convolution of $p_{U|S}(u|s)$ with $N(0, \sigma)$.

D. Inference algorithm

Various inference algorithms can be employed to find the MAP estimate in (7), *e.g.*, Iterative Conditional Modes (ICM) [27], Graph Cuts [28], loopy belief propabation (LBP) [29], and various Markov Chain Monte Carlo (MCMC) samplers, such as Metropolis and Gibbs sampler [25]. We used in our experiments the Metropolis sampler, due to its flexibility and efficiency in this application. The Metropolis sampler starts from some initial configuration (*i.e.*, from an initial mask) and in each step it switches a randomly chosen label s_i in the current mask $\mathbf{s}$ to produce the so-called "candidate" mask $\mathbf{s}^C$. The candidate gets accepted or not based on the change in the posterior probability $P_{\mathbf{S}|\boldsymbol{\Theta}}(\mathbf{s}^C|\boldsymbol{\theta})/P_{\mathbf{S}|\boldsymbol{\Theta}}(\mathbf{s}|\boldsymbol{\theta})$, which effectively reduces to

$$r = \left(\frac{p_{\Theta_i|S_i}(\theta_i \mid 1)}{p_{\Theta_i|S_i}(\theta_i \mid 0)}\right) \exp\left\{2\alpha + 2\beta \sum_{j \in \mathcal{N}_i} (2s_j - 1)\right\} \quad (11)$$

when $s_i^C = 1$ and to $1/r$ when $s_i^C = 0$. Practically, the change is accepted if r exceeds a randomly generated number drawn from a uniform distribution on $[0, 1]$.

III. Proposed algorithm: LaSAL

Now we incorporate our MRF-based spatial modelling framework into an iterative algorithm for recovering $\mathbf{x}$ from incomplete measurements in (1), and enforcing structured support of the sparse transform coefficients. We start from the Constrained Split Augmented Lagrangian Shrinkage Algorithm (C-SALSA) of [3], [4], which has been experimentally shown to efficiently solve MRI reconstruction from compressively sampled data and extend it with the MRF-based regularization. The authors of [4] motivate solving the *constrained* problem (2) directly, as opposed of reverting to the common unconstrained form $\min_{\mathbf{x}} \frac{1}{2}||\mathbf{A}\mathbf{x} - \mathbf{y}||_2^2 + \tau\phi(\mathbf{x})$. By denoting the feasible set for the unconstrained problem in (2) as $E(\epsilon, \mathbf{A}, \mathbf{y}) = \{\mathbf{x} \in \mathbb{C}^N : \|\mathbf{A}\mathbf{x} - \mathbf{y}\|_2^2 \leq \epsilon\}$, this problem can be rewritten as

$$\min_{\mathbf{x} \in \mathbb{C}^N} \phi(\mathbf{P}\mathbf{x}) + \boldsymbol{\iota}_{E(\epsilon, \mathbf{I}, \mathbf{0})}(\mathbf{A}\mathbf{x} - \mathbf{y}) \quad (12)$$

where $\boldsymbol{\iota}_Q(q)$ is the indicator function, mapping $\mathbb{C}^M \mapsto \mathbb{R}$ and taking the value 0 when $q \in Q$ and $+\infty$ otherwise. C-SALSA algorithm in [4] is derived employing the variable splitting method followed by Augmented Lagrangian (AL). With constraint equalities $\mathbf{w} = \mathbf{x}$ and $\mathbf{v} = \mathbf{A}\mathbf{x} - \mathbf{y}$, the problem which refers to the regularization step in C-SALSA from [3] becomes

$$\mathbf{w}_{k+1} = \underset{\mathbf{w} \in \mathbb{C}^N}{\operatorname{argmin}} \left\{\phi(\mathbf{P}\mathbf{w}) + \frac{\mu_2}{2}\|\mathbf{w}' - \mathbf{w}\|_2^2\right\} \quad (13)$$

where $\mathbf{w}'$ is auxiliary variable.

In order to incorporate the estimated spatial support $\hat{\mathbf{s}}$ of the sparse coefficients according to our MRF model, and to restrict accordingly the solution to the model $\mathcal{M}_{\hat{\mathbf{s}}}$, we employ an indicator function on a convex set $\mathcal{M}_{\hat{\mathbf{s}}}$ as a regularization function ϕ in (13). In particular, let $\boldsymbol{\theta}' = \mathbf{P}\mathbf{w}'$ and define

$$\iota_{\mathcal{M}_{\hat{\mathbf{s}}}}(\boldsymbol{\theta}) = \begin{cases} 0, & \text{if } \boldsymbol{\theta} \in \mathcal{M}_{\hat{\mathbf{s}}}. \\ \infty, & \text{if } \boldsymbol{\theta} \notin \mathcal{M}_{\hat{\mathbf{s}}}. \end{cases} \quad (14)$$

Assuming that $\mathbf{P}$ is the analysis operator of a 1-tight (Parseval) frame and that $\mathbf{P}^{\mathbf{H}}\mathbf{P} = \mathbf{I}$ holds, $\mathbf{w}' = \mathbf{P}^{\mathbf{H}}(\mathbf{P}\mathbf{w}') = \mathbf{P}^{\mathbf{H}}\boldsymbol{\theta}'$. With this, the minimization in (13) becomes

$$\boldsymbol{\theta}_{k+1} = \underset{\boldsymbol{\theta} \in \mathbb{C}^D}{\operatorname{argmin}} \left\{\iota_{\mathcal{M}_{\hat{\mathbf{s}}}}(\boldsymbol{\theta}) + \frac{\mu_2}{2}\|\mathbf{P}^H(\boldsymbol{\theta}' - \boldsymbol{\theta})\|_2^2\right\} \quad (15)$$

We have that $\|\mathbf{P}^H(\boldsymbol{\theta}' - \boldsymbol{\theta})\|_2^2 = (\boldsymbol{\theta}' - \boldsymbol{\theta})^H\mathbf{P}\mathbf{P}^H(\boldsymbol{\theta}' - \boldsymbol{\theta}) = (\boldsymbol{\theta}' - \boldsymbol{\theta})^H(\boldsymbol{\theta}' - \boldsymbol{\theta}) = \|(\boldsymbol{\theta}' - \boldsymbol{\theta})\|_2^2$ where $\mathbf{P}\mathbf{P}^H$ is the orthogonal projection onto the range of $\mathbf{P}$. Therefore the solution of the problem in (15) takes the form of a proximal operator defined for the indicator function which is a projection operator $\Pi_{\mathcal{M}_{\hat{\mathbf{s}}}}(\boldsymbol{\theta}')$ given in (6). The proposed method converges in practice (as we show next) although we cannot present theoretical guarantee for the convergence at this point (the MRF prior is non-convex and the employed inference scheme for the spatial support is approximate).

By analogy with LaMP and LaSB algorithms, we name our method LaSAL from Lattice Split Augmented Lagrangian. Pseudo-code of the proposed method is listed under Algorithm 1. It differs from C-SALSA [4] only in steps from 8 till 11.

IV. Experiments

In this Section, we evaluate the proposed method on an MRI data set (brain scan) acquired on a Cartesian grid and provided by the Ghent University hospital (UZ Gent)[1], which was also used in [15], [21] and on a test image used in [18] [19]. Although the data were acquired on a Cartesian grid we simulate reconstructions with radial as well as with random sampling trajectories. All trajectories are defined as binary matrices on the Cartesian grid. Fig. 2 shows the test images and the sampling trajectories employed in the experiments. We use a nondecimated shearlet transform implemented with the method from [24] with 3 scales and 16, 8, and 4 orientation per scale, respectively. The MRF parameters were optimized empirically (α=0.05; β=0.13). We compare the results of the

[1]Data acquired in collaboration with Prof. Dr. Karel Deblaere at Radiology Department of UZ Gent.

Algorithm 1 LaSAL

Require: $k = 0, \mu_1, \mu_2 > 0, \kappa = \frac{\mu_1}{\mu_2}, \mathbf{y}, \epsilon, \mathbf{x}_0, \mathbf{w}_0, \mathbf{v}_0, \mathbf{b}_0, \mathbf{c}_0$

repeat
- $\mathbf{u} = \mathbf{y} + \mathbf{v_k} + \mathbf{b_k}$
- $\mathbf{u}' = \mathbf{w_k} + \mathbf{c_k}$
- $\mathbf{x}_{k+1} = (\mathbf{I} - \frac{\kappa}{1+\kappa}\mathbf{A}^H\mathbf{A})(\kappa\mathbf{A}^H\mathbf{u} + \mathbf{u}')$
- $\mathbf{v}' = \mathbf{A}\mathbf{x_{k+1}} - \mathbf{y} - \mathbf{b_k}$
- $\mathbf{v}_{k+1} = \Pi_{\iota_{E(\epsilon,\mathbf{I},\mathbf{0})}}(\mathbf{v}')$
- $\mathbf{w}' = \mathbf{x}_{k+1} - \mathbf{c}_k$
- $\boldsymbol{\theta}' = \mathbf{P}\mathbf{w}'$
- $\hat{\mathbf{s}} \leftarrow$ *MAP-estimation*$\{\boldsymbol{\theta}'\}$
- $\boldsymbol{\theta}_{k+1} = \Pi_{\mathcal{M}_{\hat{\mathbf{s}}}}(\boldsymbol{\theta}')$
- $\mathbf{w}_{k+1} = \mathbf{P}^H\boldsymbol{\theta}_{k+1}$
- $\mathbf{b}_{k+1} = \mathbf{b}_k - (\mathbf{A}\mathbf{x_{k+1}} - \mathbf{y} - \mathbf{v_{k+1}})$
- $\mathbf{c}_{k+1} = \mathbf{c}_k - (\mathbf{x}_{k+1} - \mathbf{w}_{k+1})$
- $k = k + 1$

until some stopping criterion is satisfied

return $\mathbf{x} = \mathbf{x}_{k+1}$

proposed LaSAL to C-SALSA [4], augmented Lagrangian method [15] and LaSB [21], all implemented with the same shearlet transform. Further on, we provide comparison with the state-of-the-art CS-MRI methods employing wavelet-tree sparsity WaTMRI [18], [19], FCSA [6] and FCSANL [13] using the original implementation of the authors (http://ranger.uta.edu/~huang/index.html). After 50 iterations the resulting PSNR values for any of the evaluated methods were not changing for more than 0.01 dB, hence we used 50 iterations as a stopping criterion for all the methods. The processing times, for a 256×256 image, using a non-optimized Matlab implementation, with Intel© Core™ i7 processor (2.4 GHz, 8GB RAM) are: LaSAL – 75 s (1.50 s per iteration, out of which 1.41 s on the support estimation); C-SALSA – 10.92 s; WaTMRI 0.79 s, FCSA 0.61 s and FCSANL 0.67 s.

The results in Fig. 3 show that introducing structure encoding via the MRF model clearly improves the performance over the original C-SALSA and SB methods, using the same sparsifying transform. Also LaSAL reaches higher peak signal to noise ratio (PSNR) compared to LaSB and hence we can deduce that allowing different a priori probabilities of labels $\alpha \neq 0$ in the MRF model and employing a slightly more complex iterative procedure is justified.

Fig. 4 – Fig. 6 show performance comparison with the alternative wavelet-tree sparsity methods WaTMRI [18], [19], FCSA [6] and FCSANL [13]. The results in Fig. 4 correspond to random sabsampling matrices. We performed experiments with six different sampling rates: 14%, 20%, 25%, 32%, 38% and 42%. For each sampling rate, ten random subsampling matrices were generated and the average PSNR values were recorded. For the sagittal MRI image (from Fig. 2, left), the proposed LaSAL outperforms the wavelet tree sparsity methods on all the sampling rates. For the second test image, LaSAL outperforms the reference methods only at sampling rates above 20% , but the difference in PSNR at those

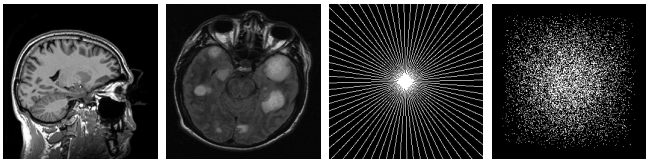

Fig. 2. Left to right: A sagittal slice from the MRI data set (256x256), a standard test image 'MRI-brain' used in [18] [19] (256x256), and examples of radial and random sampling trajectories.

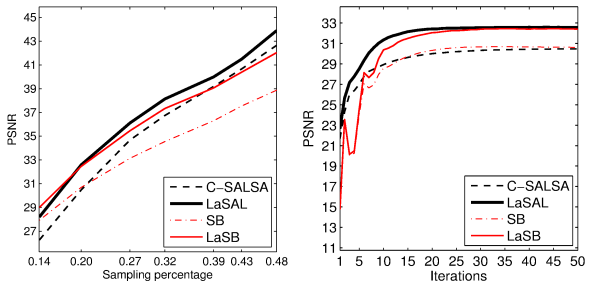

Fig. 3. Left: PSNR [dB] values of the reconstructed sagittal MRI slice using radial sampling trajectories with different sampling rates. Right: Reconstruction performances on the same image with 20% of measurements with radial trajectory.

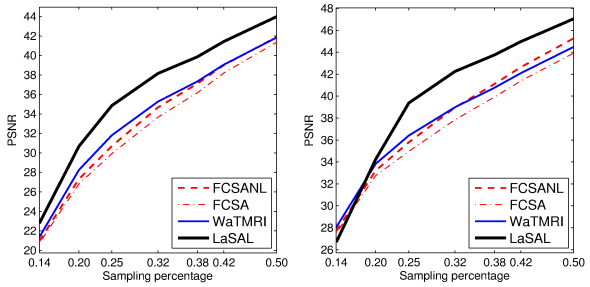

Fig. 4. PSNR [dB] values of the reconstructed sagittal MRI slice (left) and the 'MRI-brain' image (right) using random sampling trajectories with different sampling rates.

rates is significant (even more than 2dB). Fig. 5 shows the evolution of the resulting PSNR per iteration, in the case of 20% and 25% randomly chosen measurements for the two test images. Although in the first several iterations LaSAL seems unstable, it reaches stable performance afterwards and yields a significantly higher PSNR than FCASNL, FCSA and WaTMRI. The visual results in Fig. 6 demonstrate a superior performance of LaSAL, compared to wavelet tree sparsity methods, in reconstructing image details.

V. Conclusion

This work confirmed the potential of the MRF modelling framework for the recovery of compressively sampled MRI data, that was earlier hinted in [21]. Moreover, we now presented a more comprehensive study and developed a novel algorithm which incorporates the MRF modeling framework into a constrained split augmented Lagrangian method. The resulting algorithm improves upon C-SALSA in MRI reconstruction and it also outperforms the earlier method from

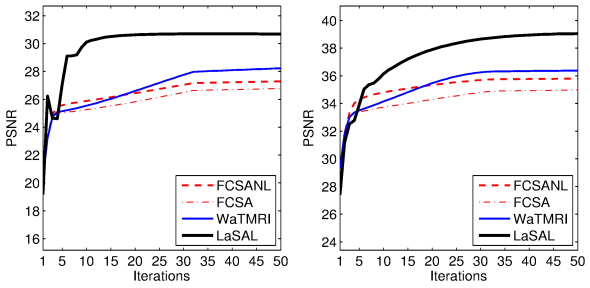

Fig. 5. PSNR [dB] values of the reconstructed sagittal MRI slice (left) and the 'MRI-brain' image (right) in 50 iterations using random sampling trajectories with 20% and 25% of measurements, respectively.

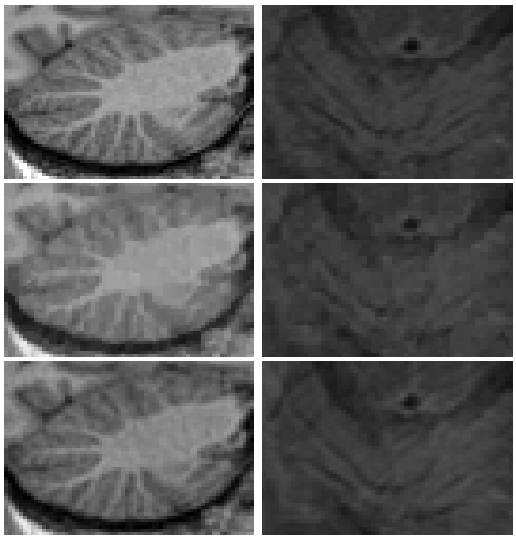

Fig. 6. Reconstruction of the sagittal MRI slice (left column) and the 'MRI-brain' image (right column) using 20% of measurements with random sampling. First row: reference ideal images. Second row: reconstructed with WaTMRI [19]. Last row: reconstructed with LaSAL.

[21]. The results also demonstrate superior performance with respect to the alternative wavelet-tree sparsity methods both in terms of quantitative performance measures and visually.

References

[1] M. Lustig, D. Donoho, and J. M. Pauly, "Sparse MRI: The application of compressed sensing for rapid MR imaging," *Magnetic Resonance in Medicine*, vol. 58, no. 6, pp. 1182–1195, 2007.

[2] M. Lustig, D. L. Donoho, J. M. Santos, and J. M. Pauly, "Compressed sensing MRI," *IEEE Signal Processing Magazine*, vol. 25, no. 2, pp. 72–82, 2008.

[3] M. V. Afonso, J. M. Bioucas-Dias, and M. A. Figueiredo, "A fast algorithm for the constrained formulation of compressive image reconstruction and other linear inverse problems," in *IEEE Internat. Conf. on Acoustics Speech and Signal Processing (ICASSP)*, 2010, pp. 4034–4037.

[4] M. V. Afonso, J. M. Bioucas-Dias, and M. A. Figueiredo, "An augmented Lagrangian approach to the constrained optimization formulation of imaging inverse problems," *IEEE Transactions on Image Processing*, vol. 20, no. 3, pp. 681–695, 2011.

[5] S. S. Chen, D. L. Donoho, and M. A. Saunders, "Atomic decomposition by basis pursuit," *SIAM Journal on Scientific Computing*, vol. 20, no. 1, pp. 33–61, 1998.

[6] J. Huang, S. Zhang, and D. Metaxas, "Efficient MR image reconstruction for compressed MR imaging," *Medical Image Analysis*, vol. 15, no. 5, pp. 670–679, 2011.

[7] S. Ma, W. Yin, Y. Zhang, and A. Chakraborty, "An efficient algorithm for compressed MR imaging using total variation and wavelets," in *IEEE Conf. on Computer Vision and Pattern Recognition, CVPR*, 2008, pp. 1–8.

[8] D. Needell and J. A. Tropp, "Cosamp: Iterative signal recovery from incomplete and inaccurate samples," *Applied and Computational Harmonic Analysis*, vol. 26, no. 3, pp. 301–321, 2009.

[9] W. Dai and O. Milenkovic, "Subspace pursuit for compressive sensing reconstruction," *IEEE Transactions on Information Theory*, vol. 55, no. 5, pp. 2230–2249, 2009.

[10] T. Blumensath, "Accelerated iterative hard thresholding," *Signal Processing*, vol. 92, no. 3, pp. 752–756, 2012.

[11] S. R. Rajani and M. Ramasubba Reddy, "An iterative hard thresholding algorithm for CS MRI," in *SPIE Medical Imaging*, 2012, pp. 83 143W1–83 143W7.

[12] A. Beck and M. Teboulle, "A fast iterative shrinkage-thresholding algorithm for linear inverse problems," *SIAM Journal on Imaging Sciences*, vol. 2, no. 1, pp. 183–202, 2009.

[13] J. Huang and F. Yang, "Compressed magnetic resonance imaging based on wavelet sparsity and nonlocal total variation," in *9th IEEE Internat. Symp. on Biomedical Imaging (ISBI)*, 2012, pp. 968–971.

[14] T. Goldstein and S. Osher, "The split Bregman method for ℓ_1-regularized problems," *SIAM Journal on Imaging Sciences*, vol. 2, no. 2, pp. 323–343, 2009.

[15] J. Aelterman, H. Q. Luong, B. Goossens, A. Pižurica, and W. Philips, "Augmented Lagrangian based reconstruction of non-uniformly subnyquist sampled MRI data," *Signal Processing*, vol. 91, no. 12, pp. 2731–2742, 2011.

[16] B. Adcock, A. C. Hansen, and B. Roman, "The quest for optimal sampling: Computationally efficient, structure-exploiting measurements for compressed sensing," *arXiv preprint arXiv:1403.6540*, 2014.

[17] R. G. Baraniuk, V. Cevher, and M. B. Wakin, "Low-dimensional models for dimensionality reduction and signal recovery: A geometric perspective," *Proceedings of the IEEE*, vol. 98, no. 6, pp. 959–971, 2010.

[18] C. Chen and J. Huang, "Compressive sensing MRI with wavelet tree sparsity," in *Advances in neural information processing systems*, 2012, pp. 1115–1123.

[19] C. Chen and J. Huang, "Exploiting the wavelet structure in compressed sensing MRI," *Magnetic Resonance Imaging*, vol. 32, no. 10, pp. 1377–1389, 2014.

[20] V. Cevher, M. F. Duarte, C. Hegde, and R. Baraniuk, "Sparse signal recovery using Markov random fields," in *Advances in Neural Information Processing Systems*, 2009, pp. 257–264.

[21] A. Pižurica, J. Aelterman, F. Bai, S. Vanloocke, Q. Luong, B. Goossens, and W. Philips, "On structured sparsity and selected applications in tomographic imaging," in *SPIE Conference on Wavelets and Sparsity XIV*, vol. 8138, 2011, pp. 81 381D–1–12.

[22] A. Kyrillidis, L. Baldassarre, M. El Halabi, Q. Tran-Dinh, and V. Cevher, "Structured sparsity: Discrete and convex approaches," in *Compressed Sensing and its Applications*. Springer, 2015, pp. 341–387.

[23] G. Kutyniok and D. Labate, "Construction of regular and irregular shearlets," *J. Wavelet Theory and Appl.*, vol. 1, pp. 1–10.

[24] B. Goossens, J. Aelterman, H. Luong, A. Pižurica, and W. Philips, "Efficient design of a low redundant discrete shearlet transform," in *IEEE Internat. Workshop on Local and Non-Local Approximation in Image Processing, LNLA*, 2009, pp. 112–124.

[25] S. Z. Li, *Markov random field modeling in image analysis*. Springer Science & Business Media, 2009.

[26] A. Pižurica, W. Philips, I. Lemahieu, and M. Acheroy, "A joint inter-and intrascale statistical model for Bayesian wavelet based image denoising," *IEEE Transactions on Image Processing*, vol. 11, no. 5, pp. 545–557, 2002.

[27] J. Besag, "On the statistical analysis of dirty pictures," *Journal of the Royal Statistical Society. Series B (Methodological)*, pp. 259–302, 1986.

[28] V. Kolmogorov and R. Zabih, "What energy functions can be minimized via graph cuts ?" *IEEE Transactions on Pattern Analysis and Machine Intelligence*, vol. 26, pp. 65–81, 2004.

[29] K. P. Murphy, Y. Weiss, and M. I. Jordan, "Loopy belief propagation for approximate inference: An empirical study," in *Proceedings of the Fifteenth conference on Uncertainty in artificial intelligence*. Morgan Kaufmann Publishers Inc., 1999, pp. 467–475.